Organic Electronics 14 (2013) 2269–2277

Contents lists available at SciVerse ScienceDirect

Organic Electronics

journal homepage: www.elsevier.com/locate/orgel

Extracting evolution of recombination zone position in sandwiched solid-state light-emitting electrochemical cells by employing microcavity effect

Ting-Wei Wang, Hai-Ching Su *

Institute of Lighting and Energy Photonics, National Chiao Tung University, Tainan 71150, Taiwan

ARTICLE INFO

Article history:
Received 6 March 2013
Accepted 29 April 2013
Available online 18 May 2013

Keywords:
Light-emitting electrochemical cells
Recombination zone
Microcavity effect

ABSTRACT

Techniques of probing for time-dependent evolution of recombination zone position in sandwiched light-emitting electrochemical cells (LECs) would be highly desired since they can provide direct experimental evidence to confirm altered carrier balance when device parameters are adjusted. However, direct imaging of recombination zones in thin emissive layers of sandwiched LECs could not be obtained easily. In this work, we propose an alternative way to extract evolution of recombination zone position in sandwiched LECs by utilizing microcavity effect. Recombination zone positions can be estimated by fitting the measured electroluminescence spectra to simulated output spectra based on microcavity effect and properly adjusted emissive zone positions. With this tool, effects of modified carrier transport and carrier injection on performance of LECs are studied and significantly altered carrier balance can be measured, revealing that microcavity effect is useful in tracing evolution of recombination zone position in sandwiched LECs.

1. Introduction

Recently, organic light-emitting diodes (OLEDs) have attracted intense attention due to their potential applications in flat-panel displays and solid-state lighting [1,2]. Compared with conventional OLEDs, solid-state light-emitting electrochemical cells (LECs) [3,4] possess several promising advantages. LECs possesses electrochemically doped regions, i.e. p-type doping near the anode and n-type doping near the cathode, which are induced by spatially separated ions under a bias. Such doped regions significantly reduce carrier injection barriers at electrodes, giving balanced carrier injection, low operating voltages, and consequently high power efficiencies. As a result, LECs generally require only a single emissive layer, which can be easily deposited by solution processes and can conveniently utilize air-stable electrodes. The emissive materials of LECs can be roughly divided into two categories: fluorescent polymers [3] and phosphorescent cationic transition metal complexes (CTMCs) [5]. Compared with polymer LECs, LECs based on CTMCs show several further advantages and have drawn much research interests in recent years [5–34]. In such devices, no ion-conducting material is needed since these CTMCs are intrinsically ionic. Furthermore, higher electroluminescent (EL) efficiencies are expected due to the phosphorescent nature of CTMCs. Green [18] and white LECs [24,34] based on Ir (III) complexes have been shown to exhibit high device efficiencies up to 40 and 15 lm/W, respectively.

To realize highly efficient LECs, spatial control of the recombination zone for reducing exciton quenching in close proximity to electrodes [35,36] would be an important issue. However, it is difficult to directly observe the recombination zone in sandwiched LECs due to their thin emissive layers (<1 μm). A feasible alternative way is direct optical probing of the recombination zone in planar LECs with much larger interelectrode gaps (up to mm) [37–43]. With this approach, several important issues affecting

* Corresponding author. Tel.: +886 6 3032121x57792; fax: +886 6 3032535.
E-mail address: haichingsu@mail.nctu.edu.tw (H.-C. Su).

1566-1199/$ - see front matter © 2013 Elsevier B.V. All rights reserved.
http://dx.doi.org/10.1016/j.orgel.2013.04.052

device performance of LECs such as cationic effects of salts [39], work functions of electrodes [41], doping processes [38,40] and recombination zone positions [42,43] were studied with clear experimental evidence. Nevertheless, these experiments were performed on planar devices using interdigitated electrodes with spacings much larger than the interelectrode spacings of sandwiched devices and the electric fields would be significantly different in magnitudes for planar and sandwiched LECs. Since ion mobility, carrier injection efficiency and carrier mobility, which affect the recombination zone position, would be field dependent, measured EL characteristics of planar LECs would not necessarily match those of sandwiched LECs. To study device physics and to further improve device performance of sandwiched LECs based on CTMCs, for which promising device efficiencies have been achieved [11,13,15,18,20,24,26,34], feasible techniques to acquire evolution of recombination zone position of sandwiched LECs under driving are highly desired. In this work, we propose a novel technique to dynamically probe recombination zone position of sandwiched LECs by utilizing microcavity effect. Microcavity structures of sandwiched LEC devices modify wavelength dependent optical outcoupling efficiencies and thus lead to tailored EL spectra when the recombination zone is moving. Hence, the recombination zone positions of sandwiched LECs can be estimated by fitting measured EL spectra to simulated EL spectra with proper emitting zone positions. With this technique, effects of carrier trapping [26,29] and carrier injection efficiency [33] on carrier balance of sandwiched LECs can be studied with clear experimental evidence. It would be useful in optimizing device efficiencies of sandwiched LECs.

2. Experiment

2.1. Materials

The emissive complex used in this study is $Ru(dtb\text{-}bpy)_3(PF_6)_2$ (where dtb-bpy is 4,4′-ditertbutyl-2,2′-bipyridine) [6]. The hole transporting material *N*,*N*′-dicarbazolyl-3,5-benzene (mCP) with a high ionization potential was utilized to impede hole injection into $Ru(dtb\text{-}bpy)_3(PF_6)_2$ emissive layer. Both $Ru(dtb\text{-}bpy)_3(PF_6)_2$ and mCP were purchased from Luminescence Technology Corp. and were used as received. The low-gap cationic fluorescent near-infrared (NIR) laser dye 3,3′-diethylthiatricarbocyanine iodide (DTTCI) [25] was utilized as the carrier trapper in $Ru(dtb\text{-}bpy)_3(PF_6)_2$ emissive layer. DTTCI was purchased from Sigma–Aldrich Co. and was used as received.

2.2. LEC device fabrication and characterization

Indium tin oxide (ITO)-coated glass substrates were cleaned and treated with UV/ozone prior to use. A poly(3,4-ethylenedioxythiophene):poly(styrene sulfonate) (PEDOT:PSS) layer was spin-coated at 4000 rpm onto the ITO substrate in air and baked at 150 °C for 30 min. For **Device III**, an mCP layer (~20 nm) was spin-coated at 5000 rpm from chlorobenzene solutions on the PEDOT:PSS layer under ambient conditions and baked at 60 °C for 6 h in a nitrogen glove box (oxygen and moisture levels below 1 ppm) while this step was skipped for **Devices I** and **II**. The emissive layers (~450 nm, as measured by profilometry) were then spin-coated at 3000 rpm from the acetonitrile solutions of complex **1** (**Devices I** and **III**) and complex **1** containing 0.1 wt.% DTTCI (**Device II**) under ambient conditions. The concentration of the solutions used for spin coating of the emissive layers is 250 mg/mL. After spin coating, the samples were then baked at 70 °C for 10 h in a nitrogen glove box, followed by thermal evaporation of a 100 nm Ag top contact in a vacuum chamber ($\sim 10^{-6}$ torr). The electrical and emission characteristics of LEC devices were measured using a source-measurement unit and a Si photodiode calibrated with the Photo Research PR-650 spectroradiometer. All device measurements were performed under a constant bias voltage (2.5 V) in a nitrogen glove box. The EL spectra were taken with a calibrated CCD spectrograph.

3. Results and discussions

Since the thickness of the organic layer of the LECs (450 nm) is comparable to the visible optical wavelength and a highly reflective metal (Ag) is used as the cathode, the emission properties of the emissive layer can be modified in such a microcavity structure, which alters the optical mode density within it and spectrally redistributes the EL spectrum. The output EL spectrum of a bottom emitting OLED device can be calculated approximately by using the following equation [44]:

$$|E_{ext}(\lambda)|^2 = \frac{T_2 \frac{1}{N}\sum_{i=1}^{N}\left[1 + R_1 + 2\sqrt{R_1}\cos\left(\frac{4\pi z_i}{\lambda} + \varphi_1\right)\right]}{1 + R_1R_2 - 2\sqrt{R_1R_2}\cos\left(\frac{4\pi L}{\lambda} + \varphi_1 + \varphi_2\right)} \times |E_{int}(\lambda)|^2$$

where R_1 and R_2 are the reflectance from the cathode and from the glass substrate, respectively, φ_1 and φ_2 are the phase changes on reflection from the cathode and from the glass substrate, respectively, T_2 is the transmittance from the glass substrate, L is the total optical thickness of the cavity layers, $|E_{int}(\lambda)|^2$ is the emission spectrum of the organic materials without alternation of the microcavity effect, $|E_{ext}(\lambda)|^2$ is the output emission spectrum from the glass substrate, z_i is the optical distance between the emitting sublayer i and the cathode. The emitting layer is divided into N sublayers and their contributions are summed up. Since the width of p-n junction estimated by capacitance measurements when p- and n-type layers were fully established was shown to be ca. 10% of the thickness of the active layer of LECs [45], the emitting layer width should not broader than tenth of the active layer thickness and thus an emitting layer width of 45 nm and $N = 45$ were estimated in optical simulation. The PL spectrum of a thin film (450 nm) of complex **1** coated on a quartz substrate was used as the emission spectrum without alternation of the microcavity effect since no highly reflective metal layer is present in this sample. Based on this simulation method, the time-dependent recombination zone location of LECs can be estimated by fitting

measured EL spectra to simulated EL spectra with proper emitting layer position.

To demonstrate extracting evolution of recombination zone location in LECs under operation by employing microcavity effect, time-dependent EL spectra of LEC devices in three different configurations were measured and were fitted to simulated results. EL characteristics of these LEC devices were measured and are summarized in Table 1. These three types of LECs have the structures shown below. **Device I:** ITO (120 nm)/PEDOT:PSS (30 nm)/complex **1** (450 nm)/Ag (100 nm), **Device II:** ITO (120 nm)/PEDOT:PSS (30 nm)/complex **1** doped with 0.1 wt.% DTTCI (450 nm)/Ag (100 nm) and **Device III:** ITO (120 nm)/PEDOT:PSS (30 nm)/mCP (20 nm)/complex **1** (450 nm)/Ag (100 nm). **Device I** is a standard LEC type that is commonly reported in literatures [5–34]. In **Device II**, a low-gap cationic fluorescent NIR laser dye DTTCI was incorporated in the emissive layer to serve as a carrier trapper, resulting in tailored carrier balance [26]. In **Device III**, a hole transporting material with a high ionization potential was used to impede hole injection and thus affected carrier balance as well [33]. Energy levels alignments [25,46–48] of **Devices I**, **II** and **III** are shown in Fig. 1. Energy levels of complex **1** were estimated by cyclic voltammetry. Time-dependent current density and brightness of **Devices I**, **II** and **III** at 2.5 V are shown in Fig. 2a–c, respectively. All LECs exhibited similar trends in time-dependent current and brightness characteristics under constant-bias operation. After the bias was applied, device current and brightness increased due to enhanced carrier injection induced by gradually formed p- and n-type doped layers near electrodes. When the doped layers were well established, both device current and brightness approach steady-state values. These results are similar to those reported for LECs based on Ru complexes [6,8]. Estimating recombination zone position by comparing measured and fitted simulated EL spectra and related discussions of each type of LEC devices are detailed in the following subsections.

3.1. LECs in a standard configuration

A standard LEC configuration consists of an emissive layer sandwiched between a PEDOT:PSS layer and Ag electrode. The energy levels of a standard LEC is depicted in Fig. 1 (**Device I**). Measured EL spectra of **Device I** at 8, 12, 18 and 58 min after a bias of 2.5 V was applied are shown in Fig. 3a–d, respectively. Time-dependent evolution of EL spectra would not be attributed to degradation of the emissive material since devices with thinner emissive layers (ca. 100 nm) exhibited relatively stable EL spectra during 10 h operation (data not shown). Such phenomena would result from modified output EL spectra in a microcavity structure [44]. In thicker devices (450 nm), enhanced output EL intensity due to constructive interference occurs at the red to NIR region and thus broadened (Fig. 3b and c) or even dual-peak (Fig. 3d) EL spectra were measured when the recombination zone moved accordingly. However, in thinner devices (ca. 100 nm), such constructive interference would take place at regions outside the emission spectrum of complex **1**, leading to relatively stable EL spectra even when the recombination zone is moving. Hence, no significant change in EL spectra during operation was observed in

Table 1
Summary of the LEC device characteristics.

Device[a]	Bias (V)	t_{max} (min)[b]	L_{max} (cd m^{-2})[c]	$\eta_{ext,\ max}$ (%)[d]	$\eta_{p,\ max}$ (lm W^{-1})[e]	$\eta_{ext,\ steady}$ (%)[f]
I	2.5	115	0.66	2.69	3.07	1.8
II	2.5	>600[g]	2.85	2.20	2.18	1.1
III	2.5	>600[g]	2.90	2.03	2.21	1.2

[a] **Device I**: ITO (120 nm)/PEDOT:PSS (30 nm)/complex **1** (450 nm)/Ag (100 nm), **Device II:** ITO (120 nm)/PEDOT:PSS (30 nm)/complex **1** doped with 0.1 wt.% DTTCI (450 nm)/Ag (100 nm) and **Device III:** ITO (120 nm)/PEDOT:PSS (30 nm)/mCP (20 nm)/complex **1** (450 nm)/Ag (100 nm).
[b] Time required to reach the maximal brightness.
[c] Maximal brightness achieved at a constant bias voltage.
[d] Maximal external quantum efficiency achieved at a constant bias voltage.
[e] Maximal power efficiency achieved at a constant bias voltage.
[f] Steady-state external quantum efficiency achieved at a constant bias voltage.
[g] Maximal brightness has not reached after 10 h operation.

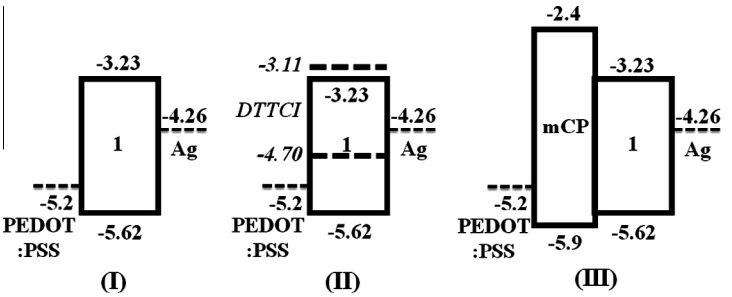

Fig. 1. Energy level diagrams of **Devices I**, **II** and **III**.

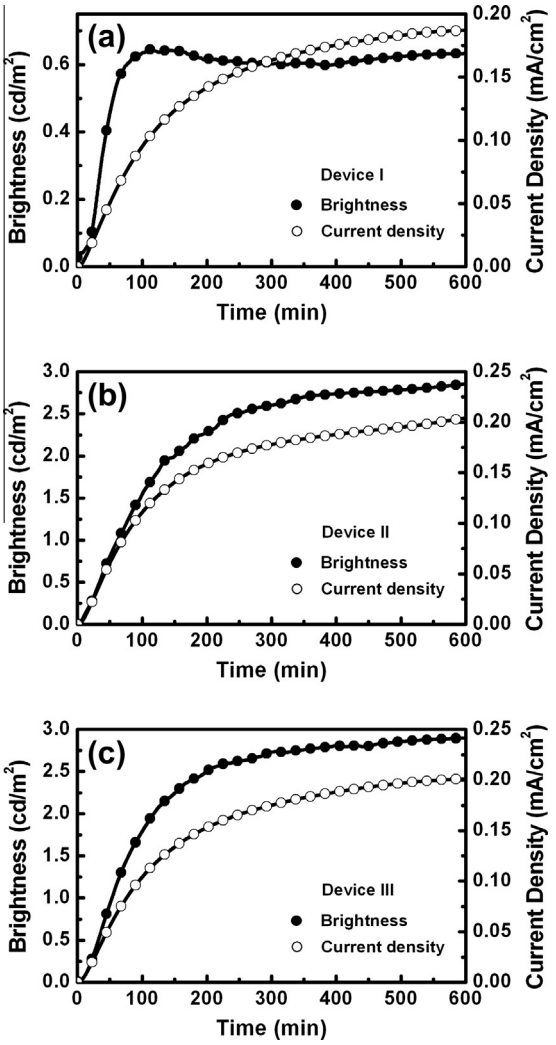

Fig. 2. Time-dependent current density (open symbol) and brightness (solid symbol) of: (a) **Device I**, (b) **Device II** and (c) **Device III** under 2.5 V.

LECs based on thin films (ca. 100 nm) of similar Ru complexes [6–8]. Simulated EL spectra were fitted to measured EL spectra by adjusting the recombination zone position (z_i) in the equation shown above. Fitted simulated EL spectra and consequently obtained recombination zone position (z_i) are separately shown in each subfigure of Fig. 3. Initially, the recombination zone was located near the cathode (z_i = 100 nm, Fig. 3a) and then gradually moved to the center of the active layer (z_i = 250 nm, Fig. 3d) after ca. 1 h operation. After 1 h, EL spectra remained relatively unchanged and thus the recombination zone position would be fixed. The trend of evolution in the recombination zone position could be understood by energy level alignments of **Device I** shown in Fig. 1. The injection barrier for hole (0.42 eV) is much lower than that for electron (1.03 eV). After a bias was applied, the required amount of accumulated ions near the anode to achieve ohmic contact for hole is smaller than that required to achieve ohmic contact for electron at the cathode. Therefore, the hole injection efficiency was higher at the early stage of formation of electrochemically doped layers and the recombination zone would locate near the cathode consequently. When both p- and n-type layers were getting well established, balanced carrier injection could be achieved and the recombination zone would move toward the center of the active layer. Further driving of LEC devices (after 1 h) results in continuous extension of the doped layers and the intrinsic layer between the doped layers shrinks [27]. The device current was thus enhanced continuously due to increased electric field in the intrinsic layer with gradually reduced thickness (Fig. 2a). With relatively stable carrier injection efficiency and spatial confinement of carrier recombination in a reduced intrinsic layer, the recombination zone position would be relatively fixed after 1 h operation.

Moving of the recombination zone also shows physical correlations with the time-dependent device efficiency. Time-dependent external quantum efficiency (EQE) of **Device I** under 2.5 V during 10 h operation is shown in the inset of Fig. 4. Compared with previously reported time-dependent device efficiencies of LECs based on thinner films (<100 nm) of similar Ru complexes [6,8], it is interesting to note that thicker **Device I** abnormally exhibited a sharp transient peak at the beginning. To clarify the physical origin of this transient peak, time-dependent EQE of **Device I** under 2.5 V for the initial 70 min of operation is shown in Fig. 4 and the corresponding evolution of recombination zone position is also shown for comparison. It is obvious that decrease of device efficiency was accompanied by moving of recombination zone and both recombination zone position and device efficiency approached steady-state values after 1 h operation. According to the proposed operating mechanism of sandwiched LECs [27], after the carrier injection barrier has been overcome, the intrinsic layer is still narrowing due to continuously extended doped layers. The excitons formed in the narrowed intrinsic layer adjacent to doped layers suffer quenching and thus device efficiency deteriorates. When the recombination zone was still moving, the doped layer was extending and continuous narrowing of the intrinsic layer resulted in decreasing of device efficiency over time (t < 1 h, inset of Fig. 4). As long as the recombination zone was relatively fixed, which implied the p-doped/intrinsic (undoped)/n-doped (p-i-n) structure was getting stable, the degree of exciton quenching would remain relatively unchanged and the device efficiency was consequently almost the same after 1 h operation (t > 1 h, inset of Fig. 4). In LECs based on thinner films (<100 nm) of similar Ru complexes [6,8], significant exciton quenching would take place at the early stage of operation since the intrinsic layer would reduce rapidly due to fast extension of doped layers. Hence, sharp transient efficiency peaks shortly after applying biases were rarely measured for thinner LEC devices. Comparison of time-dependent evolution of device efficiency and recombination zone position provides another confirmation of previously reported operating model of sandwiched LECs [27]. Furthermore, time-dependent evolution of recombination zone position would be useful in revealing effects of doping of a carrier trapper and tailoring carrier injection efficiency on carrier balance of LEC devices.

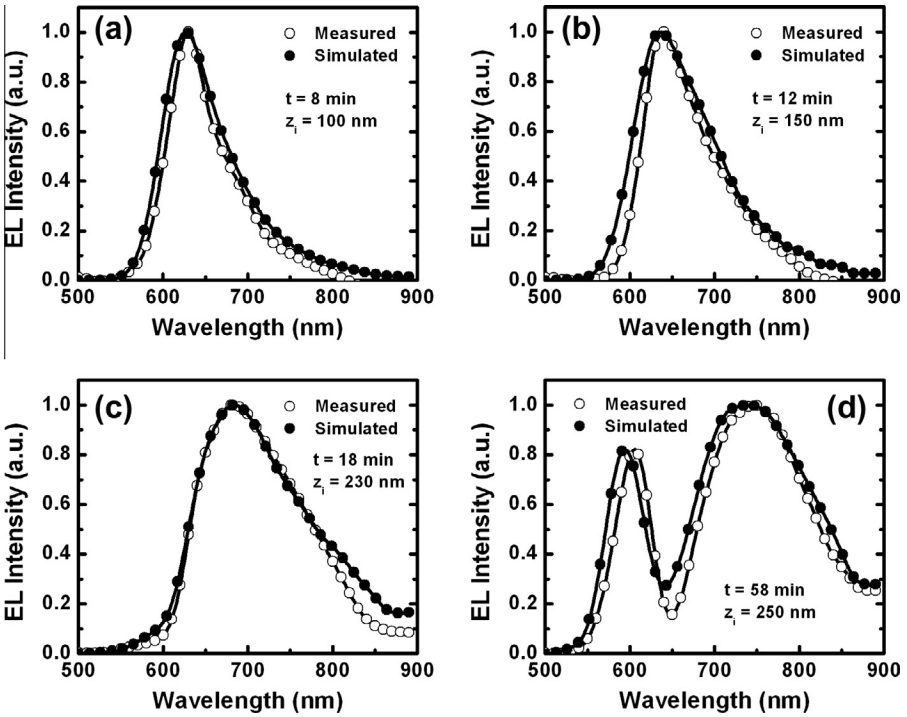

Fig. 3. Simulated (solid symbol) and measured (open symbol) EL spectra of **Device I** at (a) 8, (b) 12, (c) 18 and (d) 58 min after a bias of 2.5 V was applied. The recombination zone position (z_i) estimated from fitting of simulated and measured EL spectra is shown in each subfigure.

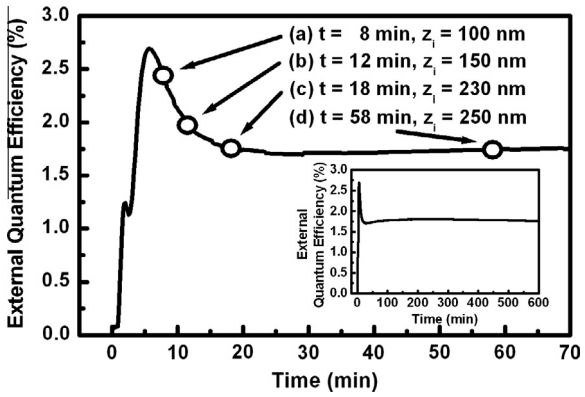

Fig. 4. Time-dependent external quantum efficiency of **Device I** under 2.5 V for the initial 70 min of operation. Time-dependent evolution of recombination zone position is shown for comparison. Inset: complete time-dependent external quantum efficiency of **Device I** for 10 h operation.

3.2. LECs doped with a carrier trapper

Doping of a carrier trapper in the emissive layer of LECs has been shown to be effective in affecting device efficiency due to significantly tailored carrier balance [26]. However, experimental evidence of modified recombination zone position resulting in affected device efficiency was not reported. In this study, a low-gap NIR carrier trapper DTTCI was doped in the LECs based on complex **1** (**Device II**). The energy level alignments of **Device II** are depicted in Fig. 1. Both the host complex **1** and the guest DTTCI possess similar lowest unoccupied molecular orbital (LUMO) level energies while they show significantly different energies in highest occupied molecular orbital (HOMO) levels. Hole trapping on the guest rather than direct hole injection onto the host would be preferred. Therefore, the guest would serve as a hole trapper in the emissive layer. Similar procedures as treated for **Device I** were performed to estimate time-dependent evolution of recombination zone position for **Device II**. As shown in Fig. 5a–d, the estimated recombination zone positions at 13, 50, 125 and 250 min after a bias of 2.5 V was applied were 390, 377, 338 and 295 nm away from the cathode. The recombination zone moved from the proximity of the anode toward the center of the emissive layer during operation. The time-dependent moving direction of the recombination zone of LECs doped with a hole trapper (**Device II**) is contrary to that of LECs based on neat films (**Device I**) (*cf.* Figs. 3 and 5). As a bias was just applied, the doped layers have not well formed yet and thus the recombination zone position was determined mainly by hole trapping induced by the low-gap guest. As the doping processes continued, enhancement in injection efficiency of hole would be faster than that of electron due to a lower hole injection barrier (**Device II,** Fig. 1). Hence, the recombination zone was then shifted toward the center of the emissive layer. When the doped layers were well established (t > 250 min), the injection efficiencies of hole and electron remained relatively unchanged and the recombination zone position was stabilized.

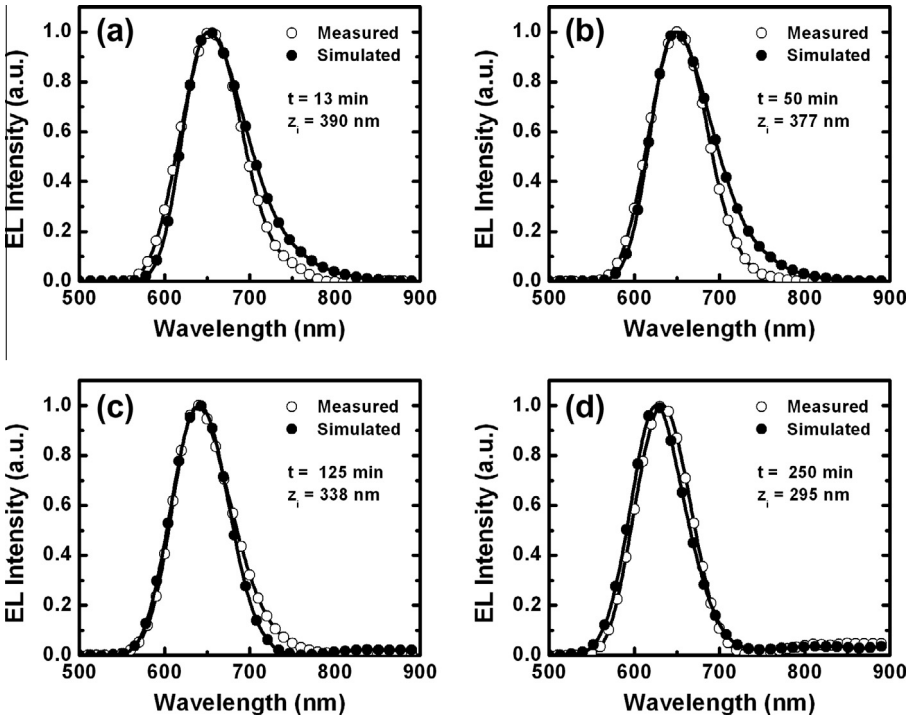

Fig. 5. Simulated (solid symbol) and measured (open symbol) EL spectra of **Device II** at (a) 13, (b) 50, (c) 125 and (d) 250 min after a bias of 2.5 V was applied. The recombination zone position (z_i) estimated from fitting of simulated and measured EL spectra is shown in each subfigure.

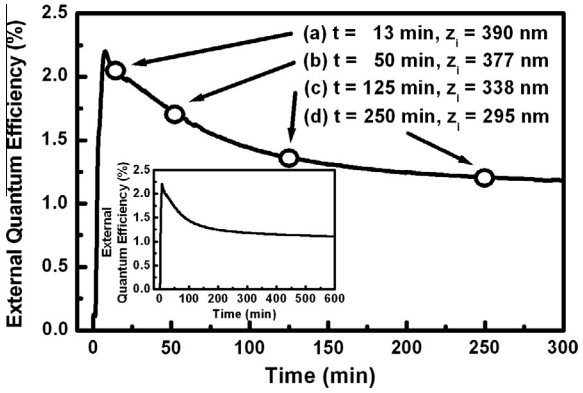

Fig. 6. Time-dependent external quantum efficiency of **Device II** under 2.5 V for the initial 300 min of operation. Time-dependent evolution of recombination zone position is shown for comparison. Inset: complete time-dependent external quantum efficiency of **Device II** for 10 h operation.

Time-dependent EQE of **Device II** under 2.5 V during 10 h operation is shown in the inset of Fig. 6. A transient EQE peak at the beginning ($t < 300$ min) was also observed in **Device II** and decrease of device efficiency was accompanied accordingly by moving of recombination zone (Fig. 6), indicating exciton quenching in recombination zone due to extension of doped layers. However, as compared to neat-film **Device I,** it took more time for doped **Device II** to reach stable device efficiencies. The time required for the brightness of **Device II** to reach the maximum value was also much longer than that of **Device I** (*cf.* Fig. 2a and b). Similar results were reported for LECs doped with low-gap guests, in which significantly lengthened turn-on times were measured [25,26]. Doping of a low-gap guest would increase the resistivity of the emissive layer due to carrier trapping. Since some voltage drop occurs in the doped layers, the effective voltage drop across the undoped layer would thus be lowered. It results in lower electric field available for driving mobile ions and slower device response consequently. Furthermore, the steady-state EQE of **Device II** (1.1%) achieved when the recombination zone was relatively fixed is significantly lower than that of **Device I** (1.8%) (*cf.* Figs. 4 and 6). It would be related to the discrepancy in stabilized recombination zone positions for these two devices. For **Device I**, the stabilized recombination zone position was close to the center of the emissive layer (250 nm away from the cathode). It ensures larger distances between the recombination zone and the doped layers and thus a lesser degree of exciton quenching would be expected. As compared to **Device I**, the stabilized recombination zone position of **Device II** was pushed toward the anode by 45 nm due to hole trapping (Fig. 6). Since the recombination zone is closer to the p-type doped layer, severer exciton quenching would take place in **Device II**, rendering deteriorated device efficiencies. These results confirm that carrier balance can be tailored by doping a carrier trapper to adjust the degree of exciton quenching and to modify the device efficiency in consequence.

3.3. LECs with a transporting layer impeding carrier injection

Tailoring carrier injection efficiency by adding a transporting layer to facilitate or to impede carrier injection has been reported to be effective in modifying device efficiencies of LECs [33]. However, the explanation of mechanisms responsible for altered device efficiencies lacked direct experimental evidence [33]. To clarify the effects of modifying carrier injection efficiency on carrier balance of LECs, a thin hole-transporting layer (20 nm) made of mCP, which exhibits a high ionization potential, was inserted between the PEDOT:PSS layer and the emissive layer to impede hole injection (**Device III**). The energy level alignments of **Device III** are shown in Fig. 1. Similar procedures as mentioned above were performed for **Device III** to estimate time-dependent evolution of recombination zone position. As shown in Fig. 7a–d, the estimated recombination zone positions at 12, 23, 58 and 175 min after a bias of 2.5 V was applied were 365, 355, 290 and 273 nm away from the cathode. The time-dependent moving direction of the recombination zone of **Device III** is the same as that of **Device II** while is contrary to that of **Device I.** With a thin transporting layer to impede hole injection, the recombination zone moved from the proximity of the anode toward the center of the emissive layer during operation. When the doped layers have not well formed yet, the amount of hole injected into the emissive layer would be significantly reduced due to a high injection barrier at the PEDOT:PSS/mCP interface (**Device III**, Fig. 1). Hence, as compared to **Device I**, the recombination zone of **Device III** at the early stage of operation was closer to the anode. As the doping processes proceeded, anions in the emissive layer would drift into the intrinsic mCP layer and result in p-type doping consequently [49]. Since the hole injection barrier gradually reduced as the doped layer developed, the amount of injected holes increased significantly and the recombination zone was shifted toward the center of the emissive layer with time. Finally, after the doped layers were well established ($t > 200$ min), the injection efficiencies of hole and electron remained relatively unchanged and the recombination zone position was stabilized.

Time-dependent EQE of **Device III** under 2.5 V during 10 h operation is shown in the inset of Fig. 8. A transient EQE peak at the beginning ($t < 200$ min) was also observed in **Device III** and decrease of device efficiency was accompanied accordingly by moving of recombination zone (Fig. 8). Since the recombination zone was moving while the doped layers were extending, these results also indicate exciton quenching in recombination zone due to extension of doped layers. However, a dip followed by a slight recovery in EQE shortly after the bias was just applied was observed for **Device III** (3–20 min, Fig. 8). This abnormal phenomenon may be attributed to altered distance between the recombination zone and the frontier of p-type doped layer at the beginning of operation. Compared to non-ionic mCP layer, the ionic mobility would be higher in ionic emissive layer and the formation speed of doped layer would also be higher in the emissive layer. Thus, shortly after the bias was applied, the speed for the p-type doped layer to extend into the center of the emissive layer would be higher than the speed for the recombination zone to move away from the anode, which would

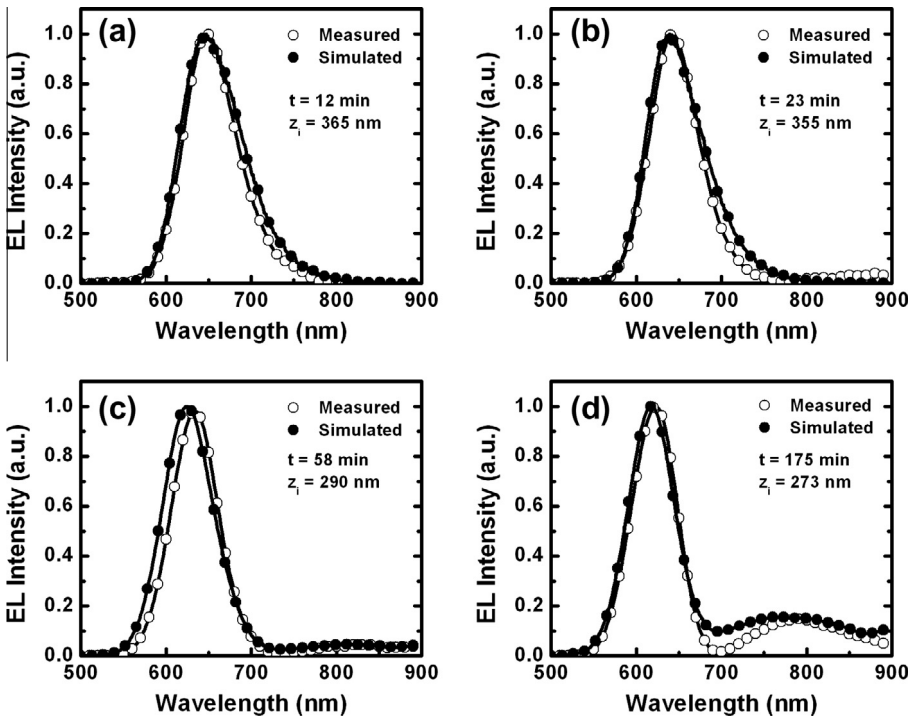

Fig. 7. Simulated (solid symbol) and measured (open symbol) EL spectra of **Device III** at (a) 12, (b) 23, (c) 58 and (d) 175 min after a bias of 2.5 V was applied. The recombination zone position (z_i) estimated from fitting of simulated and measured EL spectra is shown in each subfigure.

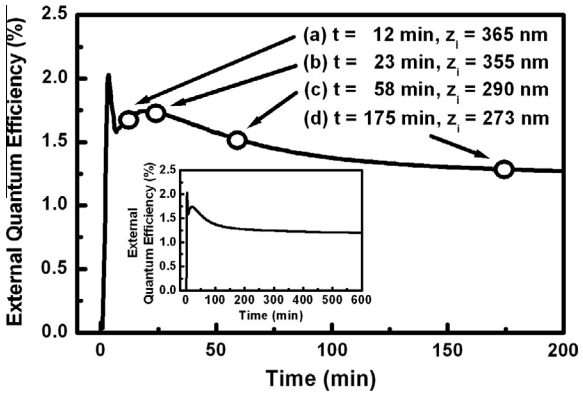

Fig. 8. Time-dependent external quantum efficiency of **Device III** under 2.5 V for the initial 200 min of operation. Time-dependent evolution of recombination zone position is shown for comparison. Inset: complete time-dependent external quantum efficiency of **Device III** for 10 h operation.

mainly result from enhanced hole injection efficiency due to formation of the p-type layer in mCP layer. The distance between the recombination zone and the frontier of p-type doped layer would reduce in consequence and significant exciton quenching would take place, leading to a rapid drop in EQE during the initial 3–6 min (Fig. 8). As the hole injection efficiency enhanced due to gradually formed p-type doped layer in mCP layer, the recombination zone would move away from the anode at an increased speed. It would increase the distance between the recombination zone and the frontier of p-type doped layer. Thus, it would result in mitigated exciton quenching and recovery in device efficiency at 6–20 min after a bias was applied. Subsequent decrease in device efficiency would be attributed to exciton quenching in recombination zone induce by further extension of doped layers. The steady-state EQE of **Device III** is 1.2%, which is lower than that of **Device I** (1.8%). The reason is similar to that mentioned for **Device II**, which also exhibited a lower EQE than **Device I.** As shown in Fig. 8, the stabilized recombination zone of **Device III** located at 273 nm away from the cathode. Compared to **Device I**, which showed a stabilized recombination zone at 250 nm away from the cathode, the recombination zone position for **Device III** was closer to the p-type doped layer and thus resulted in severer exciton quenching, rendering lowered device efficiencies. These results reveal that inserting a transporting layer to impede carrier injection is effective in altering carrier balance of LECs and device efficiencies can thus be modified.

4. Conclusions

In summary, we have demonstrated a novel method to dynamically monitor the evolution of recombination zone position of an operating sandwiched LEC by employing microcavity effect. With this tool, the recombination zone of CTMC-based LECs doped with a low-gap carrier trapper has been shown to be closer to the anode as compared to neat-film devices, leading to severer exciton quenching and deteriorated device efficiencies. Similarly, adding a hole-transporting layer with a high ionization potential to impede hole injection also resulted in a recombination zone closer to the anode. Exciton quenching took place in the recombination zone in the proximity of the anode and lower device efficiencies were obtained as well. These results provide direct experimental evidence to confirm that carrier balance of LECs can be modified by adjusting carrier transport or carrier injection. Furthermore, microcavity effect has been shown to be useful in extracting time-dependent evolution of recombination zone of sandwiched LECs, in which direct measurement of recombination zone position would be extremely difficult. The method proposed in this work would be a powerful tool for studying carrier balance of LECs.

Acknowledgement

The authors gratefully acknowledge the financial support from the National Science Council of Taiwan.

References

[1] C.W. Tang, S.A. VanSlyke, Appl. Phys. Lett. 51 (1987) 913.
[2] J. Kido, K. Hongawa, K. Okuyama, K. Nagai, Appl. Phys. Lett. 64 (1994) 815.
[3] Q. Pei, G. Yu, C. Zhang, Y. Yang, A.J. Heeger, Science 269 (1995) 1086.
[4] Q. Pei, Y. Yang, G. Yu, C. Zhang, A.J. Heeger, J. Am. Chem. Soc. 118 (1996) 3922.
[5] J.K. Lee, D.S. Yoo, E.S. Handy, M.F. Rubner, Appl. Phys. Lett. 69 (1996) 1686.
[6] S. Bernhard, J.A. Barron, P.L. Houston, H.D. Abruña, J.L. Ruglovksy, X. Gao, G.G. Malliaras, J. Am. Chem. Soc. 124 (2002) 13624.
[7] G. Kalyuzhny, M. Buda, J. McNeill, P. Barbara, A.J. Bard, J. Am. Chem. Soc. 125 (2003) 6272.
[8] J.D. Slinker, D. Bernards, P.L. Houston, H.D. Abruña, S. Bernhard, G.G. Malliaras, Chem. Commun. (2003) 2392.
[9] H. Rudmann, S. Shimada, M.F. Rubner, J. Appl. Phys. 94 (2003) 115.
[10] J.D. Slinker, A.A. Gorodetsky, M.S. Lowry, J. Wang, S. Parker, R. Rohl, S. Bernhard, G.G. Malliaras, J. Am. Chem. Soc. 126 (2004) 2763.
[11] A.B. Tamayo, S. Garon, T. Sajoto, P.I. Djurovich, I.M. Tsyba, R. Bau, M.E. Thompson, Inorg. Chem. 44 (2005) 8723.
[12] H.J. Bolink, L. Cappelli, E. Coronado, M. Grätzel, M. Nazeeruddin, J. Am. Chem. Soc. 128 (2006) 46.
[13] Q. Zhang, Q. Zhou, Y. Cheng, L. Wang, D. Ma, X. Jing, F. Wang, Adv. Funct. Mater. 16 (2006) 1203.
[14] H.-C. Su, F.-C. Fang, T.-Y. Hwu, H.-H. Hsieh, H.-F. Chen, G.-H. Lee, S.-M. Peng, K.-T. Wong, C.-C. Wu, Adv. Funct. Mater. 17 (2007) 1019.
[15] H.-C. Su, C.-C. Wu, F.-C. Fang, K.-T. Wong, Appl. Phys. Lett. 89 (2006) 261118.
[16] J.D. Slinker, J. Rivnay, J.S. Moskowitz, J.B. Parker, S. Bernhard, H.D. Abruña, G.G. Malliaras, J. Mater. Chem. 17 (2007) 2976.
[17] H.-C. Su, H.-F. Chen, F.-C. Fang, C.-C. Liu, C.-C. Wu, K.-T. Wong, Y.-H. Liu, S.-M. Peng, J. Am. Chem. Soc. 130 (2008) 3413.
[18] H.J. Bolink, E. Coronado, R.D. Costa, N. Lardiés, E. Ortí, Inorg. Chem. 47 (2008) 9149.
[19] H.-C. Su, H.-F. Chen, C.-C. Wu, K.-T. Wong, Chem. Asian J. 3 (2008) 1922.
[20] L. He, L. Duan, J. Qiao, G. Dong, L. Wang, Y. Qiu, Chem. Mater. 22 (2010) 3535.
[21] R.D. Costa, E. Ortí, H.J. Bolink, S. Graber, C.E. Housecroft, E.C. Constable, J. Am. Chem. Soc. 132 (2010) 5978.
[22] M. Mydlak, C. Bizzarri, D. Hartmann, W. Sarfert, G. Schmid, L. De Cola, Adv. Funct. Mater. 20 (2010) 1812.
[23] H.-C. Su, Y.-H. Lin, C.-H. Chang, H.-W. Lin, C.-C. Wu, F.-C. Fang, H.-F. Chen, K.-T. Wong, J. Mater. Chem. 20 (2010) 5521.
[24] H.-C. Su, H.-F. Chen, Y.-C. Shen, C.-T. Liao, K.-T. Wong, J. Mater. Chem. 21 (2011) 9653.
[25] C.-C. Ho, H.-F. Chen, Y.-C. Ho, C.-T. Liao, H.-C. Su, K.-T. Wong, Phys. Chem. Chem. Phys. 13 (2011) 17729.
[26] C.-T. Liao, H.-F. Chen, H.-C. Su, K.-T. Wong, J. Mater. Chem. 21 (2011) 17855.
[27] M. Lenes, G. Garcia-Belmonte, D. Tordera, A. Pertegás, J. Bisquert, H.J. Bolink, Adv. Funct. Mater. 21 (2011) 1581.

[28] D. Tordera, S. Meier, M. Lenes, R.D. Costa, E. Ortí, W. Sarfert, H.J. Bolink, Adv. Mater. 24 (2012) 897.
[29] C.-T. Liao, H.-F. Chen, H.-C. Su, K.-T. Wong, Phys. Chem. Chem. Phys. 14 (2012) 1262.
[30] H.-B. Wu, H.-F. Chen, C.-T. Liao, H.-C. Su, K.-T. Wong, Org. Electron. 13 (2012) 483.
[31] T. Hu, L. He, L. Duan, Y. Qiu, J. Mater. Chem. 22 (2012) 4206.
[32] R.D. Costa, E. Ortí, H.J. Bolink, F. Monti, G. Accorsi, N. Armaroli, Angew. Chem. Int. Ed. 51 (2012) 8178.
[33] C.-T. Liao, H.-F. Chen, H.-C. Su, K.-T. Wong, Phys. Chem. Chem. Phys. 14 (2012) 9774.
[34] H.-C. Su, H.-F. Chen, P.-H. Chen, S.-W. Lin, C.-T. Liao, K.-T. Wong, J. Mater. Chem. 22 (2012) 22998.
[35] K.W. Lee, J.D. Slinker, A.A. Gorodetsky, S. Flores-Torres, H.D. Abruña, P.L. Houston, G.G. Malliaras, Phys. Chem. Chem. Phys. 5 (2003) 2706.
[36] C.-Y. Liu, A.J. Bard, Appl. Phys. Lett. 87 (2005) 061110.
[37] J. Gao, J. Dane, Appl. Phys. Lett. 83 (2003) 3027.
[38] J. Gao, J. Dane, J. Appl. Phys. 98 (2005) 063513.
[39] Y. Hu, J. Gao, Appl. Phys. Lett. 89 (2006) 253514.
[40] Y. Hu, C. Tracy, J. Gao, Appl. Phys. Lett. 88 (2006) 123507.
[41] D. Hohertz, J. Gao, Adv. Mater. 20 (2008) 3298.
[42] J. Fang, P. Matyba, N.D. Robinson, L. Edman, J. Am. Chem. Soc. 130 (2008) 4562.
[43] A. Sandström, P. Matyba, L. Edman, Appl. Phys. Lett. 96 (2010) 053303.
[44] X. Liu, D. Poitras, Y. Tao, C. Py, J. Vac. Sci. Technol. 22 (2004) 764.
[45] I.H. Campbell, D.L. Smith, C.J. Neef, J.P. Ferraris, Appl. Phys. Lett. 72 (1998) 2565.
[46] A.A. Gorodetsky, S. Parker, J.D. Slinker, D.A. Bernards, M.H. Wong, G.G. Malliaras, S. Flores-Torres, H.D. Abruña, Appl. Phys. Lett. 84 (2004) 807.
[47] Y. Shao, G.C. Bazan, A.J. Heeger, Adv. Mater. 19 (2007) 365.
[48] Y. Sun, S.R. Forrest, Appl. Phys. Lett. 91 (2007) 263503.
[49] A. Sandström, P. Matyba, O. Inganäs, L. Edman, J. Am. Chem. Soc. 132 (2010) 6646.